JACS
JOURNAL OF THE AMERICAN CHEMICAL SOCIETY
Communication
pubs.acs.org/JACS

Carbon Electrodes for K-Ion Batteries

Zelang Jian, Wei Luo, and Xiulei Ji*

Department of Chemistry, Oregon State University, Corvallis, Oregon 97331-4003, United States

Supporting Information

ABSTRACT: We for the first time report electrochemical potassium insertion in graphite in a nonaqueous electrolyte, which can exhibit a high reversible capacity of 273 mAh/g. Ex situ XRD studies confirm that KC_{36}, KC_{24}, and KC_8 sequentially form upon potassiation, whereas depotassiation recovers graphite through phase transformations in an opposite sequence. Graphite shows moderate rate capability and relatively fast capacity fading. To improve the performance of carbon K-ion anodes, we synthesized a nongraphitic soft carbon that exhibits cyclability and rate capability much superior to that of graphite. This work may open up a new paradigm toward rechargeable K-ion batteries.

Demand for Li-ion batteries (LIBs) is rapidly increasing in powering electronic devices and vehicles.[1,2] However, the scarcity and rising cost of lithium resources cause a concern about the heavy reliance on LIBs.[3] This is particularly true when considering stationary applications that are indispensable for deployment of renewable energy.[2] One of the basic requirements for stationary batteries is low cost upon scaling up where the economies of scale should be applicable. This calls for alternative energy storage devices that are based on Earth-abundant elements.[4,5] Along this line, recently, Na-ion batteries (NIBs) have received renewed attention because sodium occupies 2.3 wt % in contrast to 0.0017 wt % of lithium in Earth's crust.[6−9] Rapid progress has been made on the cathode side of NIBs, where layered metal oxides[7−9] and polyanionic compounds[10−12] demonstrate encouraging capacity and cycling life. In fact, the hurdle of NIBs is on the anode side.[13] In LIBs, graphite exhibits a reversible capacity of ∼370 mAh/g by forming LiC_6, the stage-one Li−graphite intercalation compound (Li-GIC).[14,15] Unfortunately, Na/graphite cells only deliver a maximum capacity of ∼35 mAh/g by forming NaC_{64} unless solvent molecules are coinserted or expanded graphite is used.[16−18]

Pure graphite's failure in NIBs may have discouraged progress in using graphite as an electrode in K-ion batteries (KIBs). Electrochemical potassium insertion into graphite was conducted in molten KF or KF/AlF_3 at above 700 °C.[19,20] Wang et al. reported reversible electrochemical insertion of potassium into nongraphitic carbon nanofibers at room temperature.[21] In fact, KC_8, the stage-one K-GIC, as the first discovered alkali metal GIC, has been readily synthesized by potassium vapor transport or by soaking graphite in a nonaqueous solution with potassium metal solvated.[22−25] Surprisingly, it remains unknown whether K-GICs can be formed in an electrochemical K/graphite cell at room temperature. Like NIBs, the interest in KIBs originates from the abundance of potassium because it occupies 1.5 wt % of Earth crust. Progress has been made on the cathode side of KIBs with Prussian blue and its analogues in both aqueous and nonaqueous electrolytes.[26,27]

Here, we for the first time report on the electrochemical potassium storage properties of graphite. We selected a commercially available synthetic graphite (TIMCAL TIMREX SLP50), which exhibits a well-defined crystal structure as demonstrated by X-ray diffraction (XRD), transmission electron microscopy (TEM), and Raman spectroscopy (Figures 1A and S1). The K/graphite cells are assembled in an argon-filled glovebox, with graphite as the working electrode, potassium metal (99.5%, Sigma-Aldrich) as the counter/reference electrode, and 0.8 M KPF_6 (99.5%, Sigma-Aldrich)

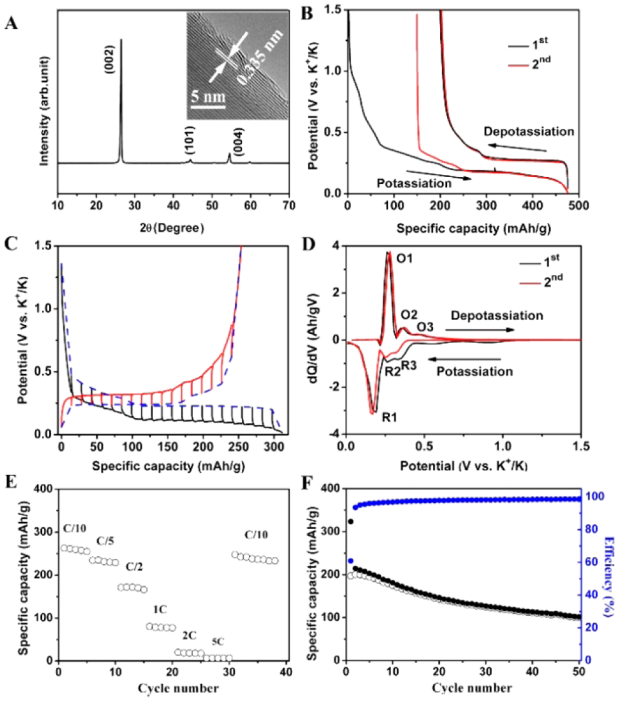

Figure 1. (A) XRD pattern of graphite. Inset: TEM image of graphite. (B) GPD profiles of graphite for the initial two cycles between 0.01 and 1.5 V at C/40. (C) GITT profiles of graphite at C/10 in the second GPD cycle. (D) dQ/dV profiles corresponding to B. (E) Rate performance and (F) Cycling performance of graphite at C/2.

Received: July 7, 2015
Published: September 2, 2015

DOI: 10.1021/jacs.5b06809
J. Am. Chem. Soc. 2015, 137, 11566−11569

in 50:50 ethylene carbonate (EC, BASF) and diethyl carbonate (DEC, BASF).

We first attempt to probe the maximum capacity of graphite in KIBs at room temperature. We conducted galvanostatic potassiation/depotassiation (GPD) tests at C/40. (We define C/1 for the current rate at which the stoichiometry of KC_8 forms during 1 h of potassiation of carbon electrodes.) Graphite exhibits surprisingly high capacities of 475 and 273 mAh/g in potassiation and depotassiation, respectively (Figure 1B). The depotassiation capacity is very close to the theoretical value of 279 mAh/g when KC_8 forms. The initial potassiation capacity is much larger than the theoretical capacity, which is responsible for the low initial Coulombic efficiency (CE) of 57.4%. Comparing potassiation potential profiles in the first two cycles shows that the slope region from 1 to 0.4 V only exists in the first cycle, which disappears in the second cycle. (All potentials are vs K^+/K.) This is very similar to the first-cycle behavior of graphite anode in LIBs when solid electrolyte interphase (SEI) forms on the graphite surface.[28,29] The following less steep slope from 0.4 to 0.2 V in the first potassiation also contributes to the initial irreversible capacity as it is much diminished in the second cycle. On the other hand, the depotassiation potential profiles overlap very well in the first two cycles.

At C/40, the primary potassiation and depotassiation plateaus locate at 0.17 and 0.27 V, respectively, thus resulting in a polarization of 0.1 V. To reveal the equilibrium potential of potassium storage, we employed galvanostatic intermittent titration technique (GITT), where a constant current of C/10 is applied for 0.5 h before cells rest at open circuit for 1 h. As Figure 1C shows, the quasi-equilibrium potentials for both potassiation and depotassiation are close to 0.24 V, much higher than that of Li insertion in graphite at ~0.1 V vs Li^+/Li.[15] The higher potassiation potential is practically critical because it relieves the risk of the dendrite formation on graphite surface. Besides the primary plateau, there exist other minor plateaus in GPD profiles, which are more evident in the differential capacity (dQ/dV) profiles, i.e., O2/R2 and O3/R3 peaks (Figure 1D).

To reveal the potassium storage mechanism in graphite, we carried out ex situ XRD for selected states of charge (SOCs) in the first-cycle GPD at C/10 (Figure 2A,B). Upon potassiation, graphite diffraction peaks do not vanish until a certain point between 0.3 and 0.2 V, where new peaks at 22.0 and 29.4° appear, which are attributed to KC_{36}, the stage-three K-GIC (point 4). In KC_{36}, one layer of potassium appears in every third pair of host graphenes (Figure 2C).[30] Upon further potassiation, KC_{36} transforms to KC_{24}, the stage-two K-GIC, where new peaks at 20.2 and 30.6° are observed (point 5). Finally, after going through a two-phase period (points 6 and 7) to 0.01 V, phase-pure KC_8, the stage-one K-GIC, forms with characteristic XRD peaks at 16.4 and 33.4°. Similar to KC_8 formed by vapor intercalation, the electrochemically formed KC_8 also shows a golden color (Figure S2). Despite the volume expansion by ~61%, a full GPD cycle does convert KC_8 back to graphite via phase transformations in an opposite direction. The ultimate potassiation product of KC_8 leads a plateau well above the plating potential of potassium metal, which may relieve the danger of dendrite formation. The lowered intensity of broadened XRD peaks of graphite after depotassiation suggests a certain degree of structural damage to graphite caused by the potassium insertion. Interestingly, a shoulder peak near the (002) peak appears upon initial potassiation and disappears at deep potassiation but shows up again after

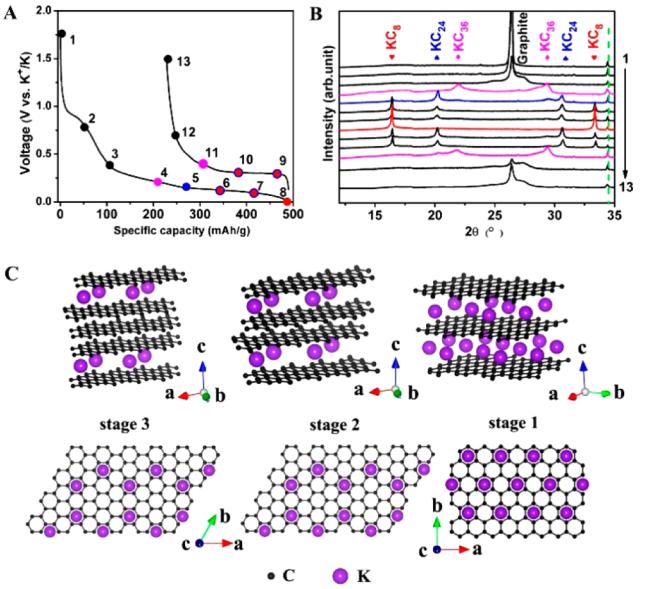

Figure 2. (A) First-cycle GPD potential profiles at C/10. (B) XRD patterns of electrodes corresponding to the marked SOCs in A. (C) Structure diagrams of different K-GICs, side view (top row) and top view (bottom row).

depotassiation beyond the stage-three phase. Further research is being conducted to reveal the phase(s) that corresponds to this shoulder peak. The ex situ XRD results for the first time show the staging-behavior of K-GICs in a K/graphite cell.

Graphite can exhibit a large capacity at low current rates, but its capacity drops dramatically upon high rates, as capacities of 263, 234, 172, and 80 mAh/g are obtained at C/10, C/5, C/2, and C/1, respectively (Figure 1E). Unfortunately, over 50 cycles at C/2, the capacity of graphite fades from 197 to 100 mAh/g (Figure 1F). In cycling, we also notice that the CE promptly increases to 93.5% in the second cycle and eventually stabilizes at ~99%. This phenomenon of rising CE values indicates the SEI formation during the initial cycling.

Looking at the capacity fading of graphite, we hypothesize that it may be related to the dramatic volume expansion of the compact graphite structure. It is intriguing to test a carbon with a less compact structure, i.e., of a much lower density. Along this line, soft carbon is best suited to test this hypothesis because its less crystalline structure exhibits a much lower density than graphite. We synthesized a soft carbon by pyrolysis of an organic aromatic compound, 3,4,9,10-perylene-tetracarboxylicacid-dianhydride (PTCDA), where the planar aromatic molecules are stacked into a highly crystalline monoclinic structure (Figure S3). The aromaticity of PTCDA certainly helps its graphitizability because annealing at 1600 °C induces a well-defined graphitic order (Figure S4).

We investigate the performance of a representative soft carbon, pyrolyzed PTCDA annealed at 900 °C. This temperature is high enough to remove most of noncarbon elements in PTCDA but low enough not to crystallize the carbon structure. Most importantly, this carbon exhibits a low density of 1.6 versus 2.3 g/cm^3 of graphite. Compared to that of graphite, the (002) XRD peak of soft carbon is much broadened (Figure 3A), which shifts to a lower angle, revealing a larger average d spacing of 0.355 nm. A representative TEM image reveals the turbostratic structure of this soft carbon (Figure S5). The corresponding selected area electron diffraction (SAED)

DOI: 10.1021/jacs.5b06809
J. Am. Chem. Soc. 2015, 137, 11566−11569

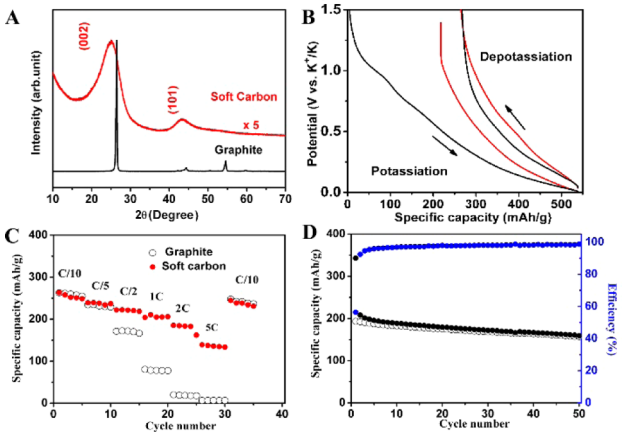

Figure 3. (A) XRD pattern of soft carbon compared with that of graphite. (B) GPD profiles of soft carbon for the initial two cycles between 0.01 and 1.5 V at C/40. Red curves are from the second cycle. (C) Rate performance of soft carbon and (D) Cycling performance of soft carbon at 2C.

presents halo rings, indicating its polycrystalline nature with a short-range order (inset of Figure S5). Wide bands and high intensity ratio of D-band over G-band in its Raman spectrum corroborate the less graphenic carbon structure (Figure S6).

Compared to graphite, soft carbon exhibits very different GPD potential profiles where only slopes exist instead of plateaus, as shown in Figure 3B, which is also observed in sodiation of soft carbon. The cause for sloping instead of forming a plateau is under investigation. This carbon also exhibits a high depotassiation capacity of 273 mAh/g at C/40, an interesting coincidence because this is the same as graphite. The rate capability of soft carbon is very impressive (Figure 3C). At C/1 and C/2, soft carbon exhibits very high capacities of 210 and 185 mAh/g, respectively, compared with 264 mAh/g at C/10. Even at 5C (1395 mA/g), the soft carbon still retains a capacity of 140 mA/g. All GPD potential profiles at different rates show the similar slope behavior (Figure S7). Such high-rate behavior is comparable to the best rate capability of carbon materials in NIBs.[18,31] In contrast to the fast capacity fading of graphite anode, soft carbon exhibits much improved cyclability with a capacity retention of 81.4% after 50 cycles at 2C (Figure 3D). Its CE value increases from 56.4% in the first cycle to 92.4% in the second cycle and eventually stabilizes at ~99%. In terms of capacity fading for both K/graphite and K/soft carbon cells, the fading mechanism of carbon electrodes in KIBs is currently unclear; however, it may be related to the decomposition of the electrolyte during the repetitive potassium metal plating and stripping processes. We opened K-graphite cells after 50 cycles and observed that the separator turns yellowish (Figure S8). In future work, electrolyte optimization and prepotassiation of carbon anodes will be carried out to improve the cycling performance and CEs.

We for the first time reveal that potassium can be reversibly inserted into graphite with a high capacity of 273 mAh/g in electrochemical cells. Revealed by ex situ XRD, we discovered that upon potassiation the stage-one KC_8 forms via stage-three KC_{36} and stage-two KC_{24} as intermediate phases where the phase transformations are reversible in converting KC_8 back to a less crystalline graphite. Graphite in KIBs suffers fast capacity fading and moderate rate capability, which may be due to the large volume change over cycling. To further improve the performance, we investigated a low-density soft carbon as a KIB anode, which exhibits much improved cycling life and very high rate capability. The new results fill important knowledge gaps on carbon electrodes in alkali metal ion batteries and may open up a completely new paradigm for energy-storage solutions.

■ ASSOCIATED CONTENT

Supporting Information

The Supporting Information is available free of charge on the ACS Publications website at DOI: 10.1021/jacs.5b06809.

Experimental section; additional data from Raman, XRD, and TEM; digital photos; molecular structure of PTCDA; and potassiation/depotassiation potential profiles at various rates. (PDF)

■ AUTHOR INFORMATION

Corresponding Author

*david.ji@oregonstate.edu

Notes

The authors declare no competing financial interest.

■ ACKNOWLEDGMENTS

We acknowledge the financial support from Oregon State University and Advanced Research Projects Agency-Energy (ARPA-E), Department of Energy of the United States, Award number: DE-AR0000297TDD. We thank Mr. Clement Bommier, Dr. Wenze Han, and Dr. Yang Sun for their discussion. We thank Professor Michael M. Lerner for providing the graphite samples and discussion. We are grateful to Professor Douglas A. Keszler for ex situ XRD measurements and Professor Chih-Hung Chang for Raman measurements.

■ REFERENCES

(1) Nagaura, T.; Tozawa, K. In *Progress in Batteries and Solar Cells*; JEC Press: Brunswick, OH, 1990; Vol. *9*, p 209.

(2) Dunn, B.; Kamath, H.; Tarascon, J.-M. *Science* **2011**, *334*, 928.

(3) Tarascon, J.-M. *Nat. Chem.* **2010**, *2*, 510.

(4) Lin, M.-C.; Gong, M.; Lu, B.; Wu, Y.; Wang, D.-Y.; Guan, M.; Angell, M.; Chen, C.; Yang, J.; Hwang, B.-J.; et al. *Nature* **2015**, *520*, 5.

(5) Liang, Y.; Chen, Z.; Jing, Y.; Rong, Y.; Facchetti, A.; Yao, Y. *J. Am. Chem. Soc.* **2015**, *137*, 4956.

(6) *Rare Earth Elements—Critical Resources for High Technology*; U.S. Geological Survey Fact Sheet 087-02; U.S. Geological Survey, Department of the Interior: Washington, DC, 2002. http://pubs.usgs.gov/fs/2002/fs087-02/.

(7) Berthelot, R.; Carlier, D.; Delmas, C. *Nat. Mater.* **2011**, *10*, 74.

(8) Xia, X.; Dahn, J. R. *Electrochem. Solid-State Lett.* **2012**, *15*, A1.

(9) Yabuuchi, N.; Kajiyama, M.; Iwatate, J.; Nishikawa, H.; Hitomi, S.; Okuyama, R.; Usui, R.; Yamada, Y.; Komaba, S. *Nat. Mater.* **2012**, *11*, 512.

(10) Jian, Z.; Zhao, L.; Pan, H.; Hu, Y.-S.; Li, H.; Chen, W.; Chen, L. *Electrochem. Commun.* **2012**, *14*, 86.

(11) Wang, L.; Lu, Y.; Liu, J.; Xu, M.; Cheng, J.; Zhang, D.; Goodenough, J. B. *Angew. Chem., Int. Ed.* **2013**, *52*, 1964.

(12) William, A., III *Energy Environ. Sci.* **2015**, *8*, 540.

(13) Yabuuchi, N.; Kubota, K.; Dahbi, M.; Komaba, S. *Chem. Rev.* **2014**, *114*, 11636.

(14) Fong, R.; von Sacken, U.; Dahn. *J. Electrochem. Soc.* **1990**, *137*, 2009.

(15) Ohzuku, T.; Iwakoshi, Y.; Sawai, K. *J. Electrochem. Soc.* **1993**, *140*, 2490.

(16) Asher, R.; Wilson, S. *Nature* **1958**, *181*, 409–410.

(17) Ge, P.; Fouletier, M. *Solid State Ionics* **1988**, *28-30*, 1172.

(18) Wen, Y.; He, K.; Zhu, Y.; Han, F.; Xu, Y.; Matsuda, I.; Ishii, Y.; Cumings, J.; Wang, C. *Nat. Commun.* **2014**, *5*, 4033.

(19) Liu, D.; Yang, Z.; Li, W. *J. Electrochem. Soc.* **2010**, *157*, D417.

DOI: 10.1021/jacs.5b06809
J. Am. Chem. Soc. 2015, 137, 11566–11569

(20) Liu, D.; Yang, Z.; Li, W.; Qiu, S.; Luo, Y. *Electrochim. Acta* **2010**, *55*, 1013.
(21) Liu, Y.; Fan, F.; Wang, J.; Liu, Y.; Chen, H.; Jungjohann, K. L.; Xu, Y.; Zhu, Y.; Bigio, D.; Zhu, T.; Wang, C. *Nano Lett.* **2014**, *14*, 3445.
(22) Schleede, A.; Wellmann, M. *Z. Kristallogr. - Cryst. Mater.* **1932**, *83*, 148.
(23) Viculis, L. M.; Mack, J. J.; Mayer, O. M.; Hahn, H. T.; Kaner, R. B. *J. Mater. Chem.* **2005**, *15*, 974.
(24) Mizutani, Y.; Abe, T.; Inaba, M.; Ogumi, Z. *Synth. Met.* **2001**, *125*, 153.
(25) Mizutani, Y.; Abe, T.; Ikeda, K.; Ihara, E.; Asano, M.; Harada, T.; Inaba, M.; Ogumi, Z. *Carbon* **1997**, *35*, 61.
(26) Eftekhari, A. *J. Power Sources* **2004**, *126*, 221.
(27) Wessells, C. D.; Peddada, S. V.; Huggins, R. A.; Cui, Y. *Nano Lett.* **2011**, *11*, 5421.
(28) Peled, E. *J. Electrochem. Soc.* **1979**, *126*, 2047.
(29) Winter, M.; Besenhard, J. O.; Spahr, M. E.; Novak, P. *Adv. Mater.* **1998**, *10*, 725.
(30) Chacón-Torres, J. C.; Wirtz, L.; Pichler, T. *Phys. Status Solidi B* **2014**, *251*, 2337.
(31) Bommier, C.; Ji, X. *Isr. J. Chem.* **2015**, *55*, 486.

DOI: 10.1021/jacs.5b06809
J. Am. Chem. Soc. 2015, 137, 11566−11569